Solid State Phenomena
ISSN: 1662-9779, Vol. 388, pp 39-45
doi:10.4028/p-L9atJa

Submitted: 2025-12-19
Revised: 2026-02-11
Accepted: 2026-02-18
Online: 2026-04-15

Microstructural Modification and Bendability Improvement in 1300 MPa Steel via Induction Surface Heat Treatment

Antti Kaijalainen[1,a*], Ahmed Abdelghany[2,b], Oskari Haiko[1,c], Anttu Hoikkaniemi[1,d] and Aki-Petteri Pokka[1,e]

[1]Materials and Mechanical Engineering, University of Oulu, Oulu 90570, Finland

[2]Future Manufacturing Technologies, Kerttu Saalasti Institute, University of Oulu, Nivala 85500, Finland

[a*]antti.kaijalainen@oulu.fi, [b]ahmed.abdelghany@oulu.fi, [c]oskari.haiko@oulu.fi, [d]anttu.hoikkaniemi@oulu.fi, [e]aki-petteri.pokka@oulu.fi

Keywords: bendability, hardness, induction heating, soft surface, ultrahigh-strength steel.

Abstract. This study investigates the effect of induction-based surface heat treatment on the microstructure and bendability of a commercial hot-rolled martensitic steel with a nominal strength of 1300 MPa. A rapid tempering process was applied at 500 °C and 700 °C using a pilot-scale 60 kW induction heating system, followed by water quenching. Microstructural characterization revealed that the treatment induced minor changes near the subsurface without affecting the centerline. The as-rolled condition exhibited the highest subsurface hardness, whereas surface-treated samples showed progressive softening due to recovery. Three-point bending tests combined with digital image correlation demonstrated a significant improvement in bendability for heat-treated samples. The as-rolled condition fractured at 0.195 strain, while the 700 °C treated specimen did not fracture even at 0.78 strain. These findings highlight that even a modest reduction in subsurface hardness can substantially enhance the formability of ultra-high-strength steels, offering a promising approach for industrial applications requiring high strength and improved bendability.

Introduction

For ultrahigh-strength strip steels (UHSS), cold bending is the primary forming method for applications such as containers and crane booms. Bendability is commonly determined as the minimum ratio of the punch radius to the strip thickness (R_p/t) that the steel can tolerate without the appearance of surface defects during bending to an angle of 90°. Digital Image Correlation (DIC) is used in this work to measure the strain distributions on the outer curvature [1–4] rather than at a 90° angle in order to study the bendability of a UHSS grade using 3-point bending tests. Shear bands have been observed to initiate near the surface at angles of approximately 45° to the surface, i.e., in the maximum shear stress directions [5]. Previous bending studies [6, 7] have demonstrated that strain localization is the precursor to failure in the air bending of UHSS, and especially excellent bendability can be achieved with a relatively soft subsurface layer down to a depth of ~5% of the sheet thickness. Therefore, it is reasonable to assume that the bendability of the strip is controlled by its near-surface characteristics.

Induction-based heat treatment offers several advantages over conventional furnace-based methods. It enables rapid austenitization and tempering, localized energy input, and significantly reduced heating times, leading to increased energy efficiency and processing throughput [8, 9]. Moreover, such rapid heating conditions can induce favorable microstructural changes by refining the grain structure and suppressing unwanted recovery mechanisms during tempering [10]. These characteristics align well with the goals of sustainable steel processing, where improved mechanical performance must be achieved without sacrificing environmental or economic viability.

While earlier studies have shown that a softer subsurface layer can enhance bendability, these findings were based on the hot-rolling process.

The main aim of the present study is to understand how bendability can be improved by tailoring the surface layer through rapid induction tempering, and how the unique thermal characteristics of ultrafast local heating influence microstructure evolution, strain localization, and bendability without compromising other mechanical properties.

Experimental

Bending samples 8 mm thick, of the commercial hot-rolled martensitic 1300 MPa steel grade, were tested with a width of 30 mm. The rapid heat treatments were conducted using the modular 60 kW high-frequency induction-heating line at the University of Oulu research facility, Nivala, Finland. This system was selected to replicate continuous and controlled feed industrial processing, as shown in Fig. 1. The thermal cycle starts with rapid tempering at 500 °C and 700 °C, achieved at a heating rate of approximately 200 °C/s. Immediately upon reaching peak temperature, the samples were passed directly into a dedicated inline water-cooling unit integrated with the induction heating line. This continuous-quenching setup ensured rapid, uniform cooling to room temperature while maintaining uninterrupted specimen motion. The purpose of this flash heat treatment sequence was to induce a refined martensitic microstructure and achieve surface softening through rapid processing. Therefore, three materials were investigated and named as follows: (1) as-rolled, (2) surface treated at 500 °C, and (3) surface treated at 700 °C.

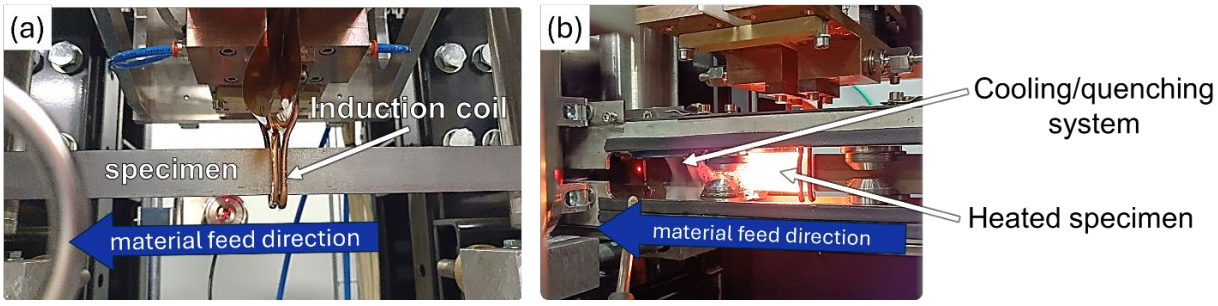

Fig. 1. Photographs of the high-speed induction heating of steel specimens using a continuous pilot-scale axial inductor system at Nivala, Finland. (a) Copper induction coil positioned above the specimen as it enters the heating zone. (b) Active heating process, where the specimen is rapidly austenitized while moving through the coil at a controlled feed rate.

General Microstructure Investigation and Hardness Measurements.

The general microstructure of the as-rolled and heat-treated materials was examined using a Keyence VK-X200 confocal laser scanning microscope. Polished specimens using 0.04 µm colloidal silica were etched with 2% Nital to reveal martensitic features, allowing assessment of the hardened case depth and structural uniformity across the cross-section. To evaluate the mechanical response through the depth, Vickers hardness measurements were performed on polished cross-sections using a Zwick/Roell ZHU2.5 universal hardness testing machine (Germany). A load of 5 kg (HV5) was applied through the thickness from top surface to bottom surface, enabling characterization of the hardness gradient resulting from the flash heat treatment. Likewise, the subsurface hardness profiles were measured using a micro-hardness tester (CSM, Switzerland) under a 1N (HV0.1) load.

Bending Trials.

The investigated materials were tested in the transverse orientation, meaning that the bend axis was perpendicular to the rolling direction. Each specimen was bent at room temperature until fracture, or until it reached the final bend angle of $\alpha = 120°$. The specimens with a width (bend length) of 30 mm were bent at room temperature using a Zwick 100 kN universal tensile test machine equipped with custom-built three-point bending tools (Fig. 2a) and a stereo DIC system. The setup enabled measurement of bending force, punch stroke, and continuous strain mapping of the outer bend surface through openings in the lower tool.

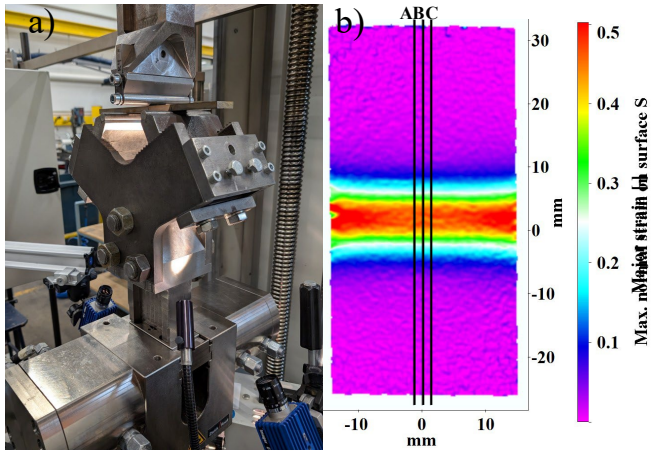

Fig. 2. a) Setup for the bending tests and DIC measurements. b) Example of a strain map from the 700 °C treated bend specimen at a 66° angle and sections A–C.

To maintain the DIC cameras focused on the measurement area, the punch remained stationary during testing, while the lower tool was displaced upward at a speed of 1 mm/s to produce the required punch stroke. A punch radius of 8 mm, die shoulder radius of 6 mm, and a die width of 90 mm (distance between shoulder centers) were used. The die shoulders were freely rotating and lubricated with PTFE spray to minimize friction. Additional details of the test setup are available in Refs. [1, 11].

The bending force was normalized by specimen width and expressed as N/mm to compensate for minor width variations. Bend angles were calculated from punch stroke data according to ISO 7438:2016, with corrections applied for the vertical elasticity of the setup (combined rigidity of the machine and tools), measured at 51.9 kN/mm.

Strain measurements were performed using a LaVision Strainmaster DIC system with two monochrome CCD cameras. The specimens were spray painted with a black-and-white speckle pattern to ensure accurate point tracking in the DIC software. The DIC recording and processing parameters are presented in Table 1. Fig. 2b provides an example of a strain map of the outer surface of a bent specimen, obtained through DIC measurement.

From the strain maps, principal strain values were extracted along three sections (A–C) positioned at the bend centerline at 1 mm intervals. The peak strain, denoted as ε_{b_max}, was calculated as the average of the maximum strain values from sections A–C at each time step.

The bending fracture strain (ε_{bf}) was defined as $\varepsilon_{b\ max}$ at the fracture angle α_f, following the procedure described in Ref. [12]. The fracture angle α_f was determined by the smallest bend angle at which $\varepsilon_{b\ max}$ exceeded 0.15, the strain rate ($d\varepsilon_{b\ max} / d\alpha$) was greater than $0.01^{\circ-1}$, and the strain acceleration ($d^2\varepsilon_{b\ max} / d\alpha^2$) surpassed $0.0003^{\circ-2}$. The threshold values were chosen with the aim of capturing the increase in strain rate that coincides with fracture, while avoiding false positives at the beginning of the test, and false negatives in cases where the crack growth (and thus strain acceleration) is very gradual. The strain rate and acceleration were calculated using the central difference method and smoothed with a seven-point moving average.

Table 1. Recording and processing parameters for the DIC system.

DIC system and software	LaVision Strainmaster (Stereo DIC), DaVis 8.4
Sensor, digitization, imaging rate	2456 × 2058, 12-bit, 2 Hz
Lens, imaging distance, image scale	35 mm C-mount, 425 mm, 25 pixels/mm
Subset size, step size, VSG	15 × 15 pixels, 5 pixels, 35 pixels
Strain window, smoothing method	5 × 5 data points, 2nd order polynomial fit
St. dev. of principal strain (noise-floor)	480 – 550 microstrain
Interpolation, shape function, algorithms	6th order spline interpolation; affine shape function; LSM (iterative least squares matching) algorithm based on optical flow estimation

Results and Discussion

Microstructure and Hardness.

Microstructural investigation revealed a fully martensitic microstructure (Fig. 3), and the surface heat treatment did not affect the centerline. Characterization showed that the fast heat treatment at 500 °C and 700 °C (i.e., the tempering effect) causes minor microstructural changes in the subsurface. Carbon diffusion to grain boundaries and the appearance of slightly coarser carbides are visible, particularly in the 700 °C sample (Fig. 3d). Red arrows in Fig. 3 (c and d) highlight representative carbide precipitates in the heat-treated subsurface regions. These microstructural features reflect the early stages of tempering and are consistent with the localized softening observed in hardness measurements.

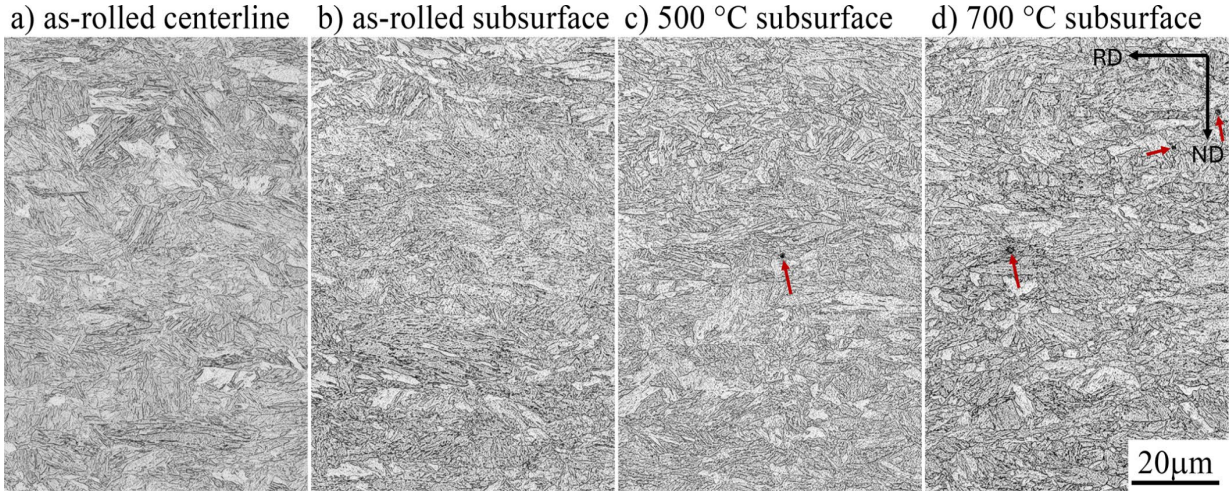

Fig. 3. Microstructural micrographs showing (a) and (b) before heat treatment; (c) and (d) after induction heat treatment under different conditions.

Fig. 4a illustrates the macrohardness profiles at different positions through the thickness. The as-rolled condition exhibits the highest average hardness (455 ± 4 HV5), followed by the material tempered at 500 °C (446 ± 7 HV5) and 700 °C (436 ± 11 HV5). The relatively uniform hardness distribution across the thickness suggests that subsequent heat treatments affected mainly near the surface, as can be seen in Fig. 4a. The reduction in hardness with increasing tempering temperature reflects the progressive softening associated with tempering processes, which promotes recovery, reduces internal stresses, and rearranges dislocations without grain growth.

Macrohardness results indicate that hardness near the subsurface exhibits noticeable variation. Hence, Fig. 4b shows microhardness profiles from 25 µm to 925 µm below the surface and centerline (CL) values. However, it should be noted that the Vickers hardness measurements are not directly comparable, as the measurements are performed with different loads. All conditions exhibit a hardness gradient, with softening near the surface and stabilization deeper into the material. This surface softening is mainly caused by the decarbonization of the surface during slab austenitization and hot rolling. The as-rolled material demonstrates the highest subsurface hardness (400 ± 18 HV0.1), while the 500 °C and 700 °C conditions show reduced values of 377 ± 16 HV0.1 and 354 ± 20 HV0.1, respectively.

The combined macro- and microhardness results demonstrate that hardness is strongly influenced by tempering temperature, which has an effect on dislocation density. The as-rolled condition retains the highest hardness due to work hardening and high dislocation density, while tempering progressively reduces hardness through recovery. These findings highlight the critical role of thermal treatments in tailoring mechanical properties for applications requiring specific strength and formability levels.

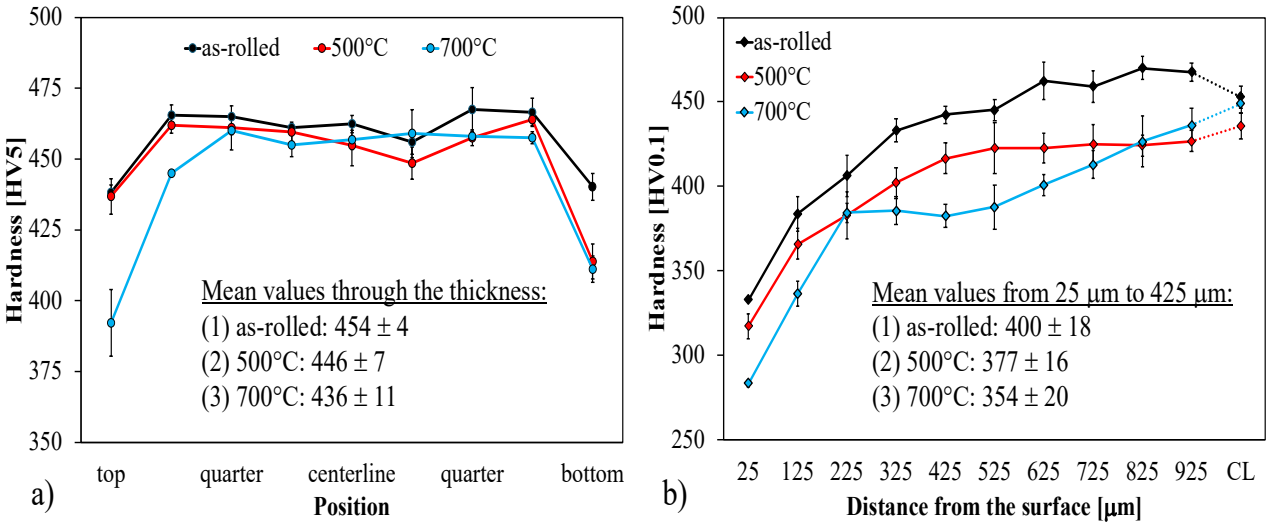

Fig. 4. a) Macrohardness and b) microhardness profiles of the investigated materials with 95% confidence limits of the means (five measurements at each thickness). Also, the mean values are given through the thickness and near the subsurface. (Vickers hardness measurements are performed with varying loads when those are not directly comparable.)

Bending.

Examples of bend samples are shown in Fig. 5, whereas Fig. 6 illustrates the evolution of the minor and major strains during bending tests, as measured by DIC at the peak strain location on the specimen surface. Evidently, the sample width was too narrow for the bending trials to achieve plane-strain condition. Generally, the width-to-thickness ratio should be at least 8, to achieve plane-strain condition, while in this case it was only 3.75.

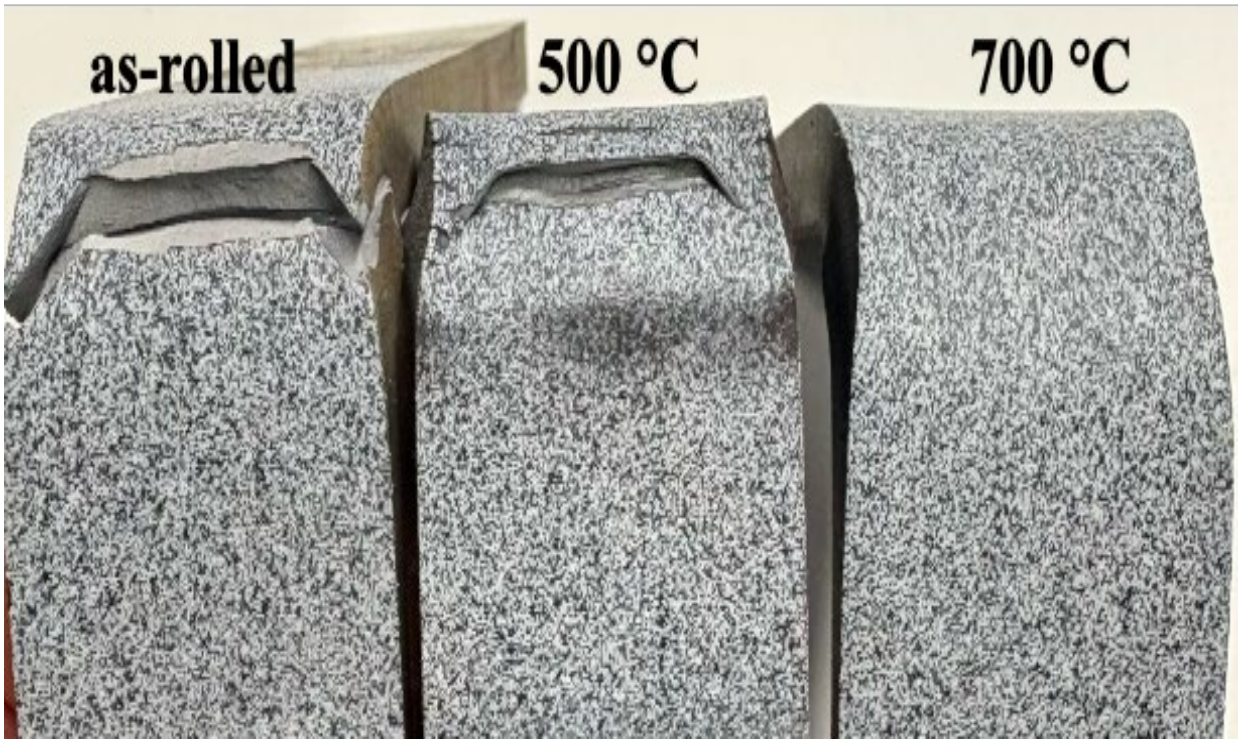

Fig. 5. Bending test samples with the bend axis transverse to the rolling direction.

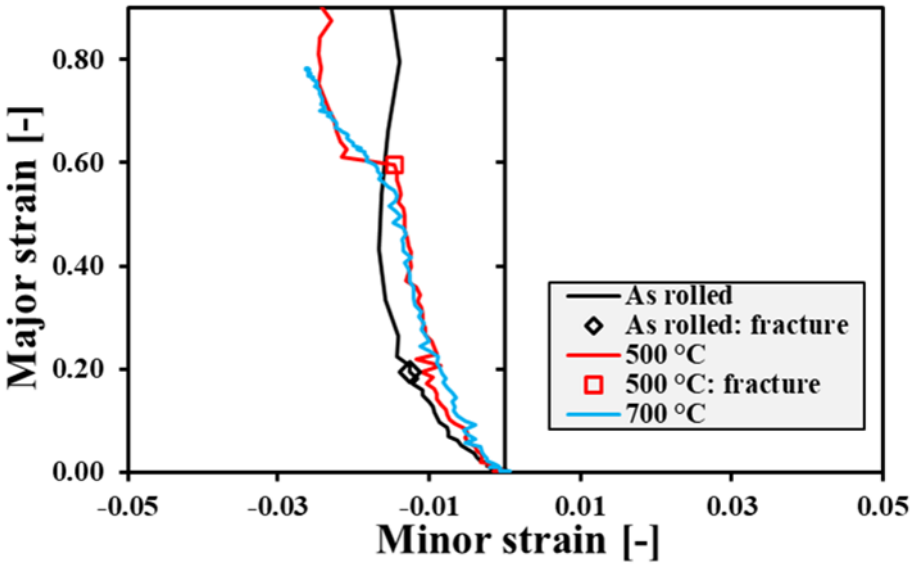

Fig. 6. Major and minor strain evolution of the bending tests.

Nevertheless, the measured normalized bending force and the peak strain $\varepsilon_{b\ max}$ are plotted against the bend angle in Fig. 7. The determined bending fracture angles and strains are listed in Table 2. The bending force of as-rolled material is higher than the heat-treated samples (Fig. 7a), indicating higher strength, as expected based on the average hardness comparison. Notably, the ε_{b_max} evolution is near identical between all the specimens until around 30° bend angle, when the as-rolled specimen starts to fracture, indicated by the sharp increase in peak strain (Fig. 7b).

The as-rolled tests clearly have the poorest bendability, as the fracture angle was 31° and fracture strain 0.195. Whereas the 500 °C surface heat-treated started to fracture first at approx. 72° angle or 0.611 strain. Surprisingly, the higher 700 °C surface heat treatment with a softer subsurface did not fracture even at 120° bending angle and ε_{b_max} above 0.78. Therefore, the 5% softer subsurface layer is enough to improve the bendability, as shown in Ref. [7].

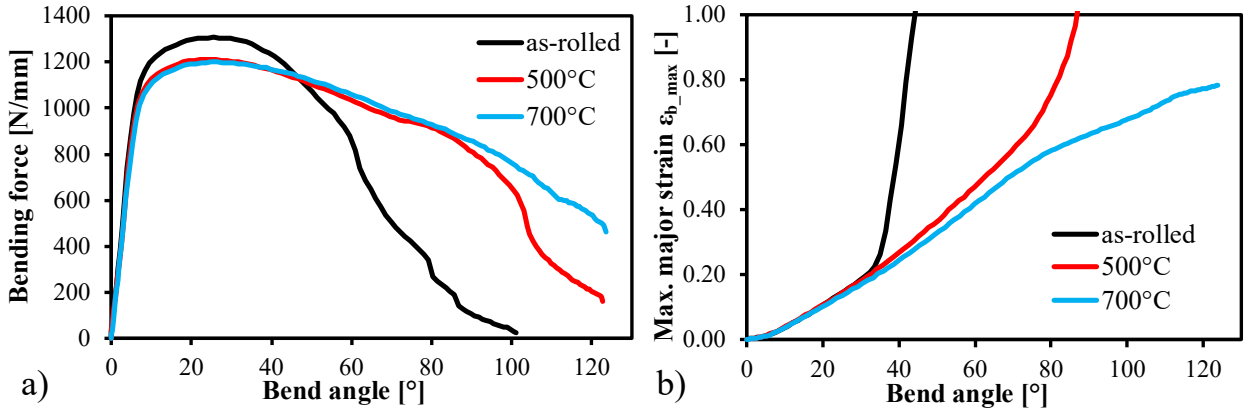

Fig. 7. Development of a) the bending force and b) the peak strain on the outside surface.

Table 2. Bending fracture angles (α_f) and fracture strains (ε_f) of the investigated specimens.

Material	α_f [°]	ε_f [-]
as-rolled	30.9	0.195
500 °C surface heat-treated	72.0	0.611
700 °C surface heat-treated	-	-

Summary

The aim of this study was to show the effect of rapid surface heating on the subsurface hardness and the three-point bending of 1300 MPa ultrahigh-strength steel. Microstructural analysis showed that the treatment caused minor changes near the subsurface without affecting the centerline, while hardness measurements showed a slight reduction in subsurface hardness with increasing tempering temperature. Therefore, the mean hardness of near subsurface (from 25 μm to 925 μm below the surface) decreased from 400 HV0.1 to 354 HV0.1. The bendability of the softer surface material improved, and no fracture was observed compared to identical steel specimens without induction treatment. These results confirm that even modest subsurface softening can substantially enhance the bendability of ultra-high-strength steels.

Acknowledgement

Financial assistance of the Business Finland project FOSSA2-Fossil-Free Steel Applications: Phase 2-is acknowledged.

References

[1] A.-P. Pokka, A.-M. Arola, A. Kaijalainen, V. Kesti, J. Larkiola, Strain distribution during air bending of ultra-high strength steels, Proc. ESAFORM 2021 (2021).

[2] A.-M. Arola, A. Kaijalainen, V. Kesti V, A.-P. Pokka, J. Larkiola, Digital image correlation and optical strain measuring in bendability assessment of ultra-high strength structural steels, Procedia Manuf. 29 (2019) 398–405.

[3] M. Kaupper, M. Merklein, Bendability of advanced high strength steels-A new evaluation procedure, CIRP Ann. Manuf. Technol. 62 (2013) 247–250.

[4] K. Cheong, C. Butcher, J. Dykeman, The influence of the through-thickness strain gradients on the fracture characterization of advanced high-strength steels, SAE Int. J. Mater. Manuf. 11 (2018) 541–552.

[5] D. Rèche, T. Sturel, O. Bouaziz O, A. Col, A.F. Gourgues-Lorenzon, Damage development in low alloy TRIP-aided steels during air-bending, Mater. Sci. Eng. A 528 (2011) 5241–5250.

[6] A. Kaijalainen, P. Suikkanen, L. Karjalainen, D. Porter, Influence of subsurface microstructure on the bendability of ultrahigh-strength strip steel, Mater. Sci. Eng. A 654 (2016) 151–160.

[7] A. Kaijalainen, M. Liimatainen, V. Kesti, J. Heikkala, T. Liimatainen, D. Porter, Influence of composition and hot rolling on the subsurface microstructure and bendability of ultrahigh-strength strip, Metall. Mater. Trans. A 47 (2016) 4175–4188.

[8] N.S. Kim, G.G. Kang, An investigation of flow characteristics considering the effect of viscosity variation in the thixoforming process, J. Mater. Process. Technol. 103 (2000) 237–246.

[9] H.K. Jung, The induction heating process of semi-solid aluminium alloys for thixoforming and their microstructure evaluation, J. Mater. Process. Technol. 105 (2000) 176–190.

[10] A. Kaijalainen, O. Haiko, S. Sadeghpour, V. Javaheri, J. Kömi, The influence of rapid tempering on the mechanical and microstructural characteristics of 51CrV4 steel, Metals 14 (2024) 60.

[11] A. Kaijalainen, A.-P. Pokka, M. Jaskari, J. Kömi, Effect of surface roughness on strain distribution during bending, IOP Conf. Ser. Mater. Sci. Eng. 1270 (2022) 012080.

[12] A.-P. Pokka, V. Kesti, A. Kaijalainen, Local formability and bendability of UHSS: Correlations between bending and tensile fracture strains. Int. J. Solids Struct. 320 (2025) 113524.a.